A wireless interrogation system exploiting narrowband acoustic resonator for remote physical quantity measurement

J.-M. Friedt, C. Droit, G. Martin, S. Ballandras

A wireless interrogation system exploiting narrowband acoustic resonator for remote physical quantity measurement

J.-M Friedt,[1,a)] C. Droit,[2] G. Martin,[2] and S. Ballandras[2]
[1]*SENSeOR, 32 Avenue de l'Observatoire, 25044 Besançon, France*
[2]*Department of Time and Frequency, FEMTO-ST, 32 Avenue de l'Observatoire, 25044 Besançon, France*

(Received 8 September 2009; accepted 3 November 2009; published online 11 January 2010)

Monitoring physical quantities using acoustic wave devices can be advantageously achieved using the wave characteristic dependence to various parametric perturbations (temperature, stress, and pressure). Surface acoustic wave (SAW) resonators are particularly well suited to such applications as their resonance frequency is directly influenced by these perturbations, modifying both the phase velocity and resonance conditions. Moreover, the intrinsic radio frequency (rf) nature of these devices makes them ideal for wireless applications, mainly exploiting antennas reciprocity and piezoelectric reversibility. In this paper, we present a wireless SAW sensor interrogation unit operating in the 434 MHz centered ISM band—selected as a tradeoff between antenna dimensions and electromagnetic wave penetration in dielectric media—based on the principles of a frequency sweep network analyzer. We particularly focus on the compliance with the ISM standard which reveals complicated by the need for switching from emission to reception modes similarly to radar operation. In this matter, we propose a fully digital rf synthesis chain to develop various interrogation strategies to overcome the corresponding difficulties and comply with the above-mentioned standard. We finally assess the reader interrogation range, accuracy, and dynamics. © *2010 American Institute of Physics.* [doi:10.1063/1.3267311]

I. BASIC PRINCIPLES

Continuous or periodic monitoring of the physical properties of industrial tools, buildings, environmental equipment, etc., provides the basic informations to replace preventive maintenance with predictive maintenance reacting to any abnormal behavior of parts of the system being monitored. However, maintenance of aging devices means embedding sensors with life expectancies longer than that of the observed system. Furthermore, the parts of interest are usually subject to harsh environmental conditions—corrosive environment, strong magnetic field associated with high current densities, or high voltages for instance—or mobile or rotating parts. Hence, wired sensors are unsuitable since the connections are often the weak point making the packaging fragile and unreliable on the long term. Battery powered wireless silicon based sensors[1] provide one solution with increasing life expectancy as lower power sensors, microcontrollers, and wireless communication interfaces are developed.[2,3] Yet, this lifetime is still finite and limited by the available battery power. Environmental preservation, however, claims for battery-less systems capable to limit pollution issues. Passive CMOS sensors based on RFID technology provide short interrogation distance and poorer temperature measurement range than those presented in this document.[4,5]

We here propose an alternative mean of monitoring chemical[6,7] and physical properties[8,9] (temperature,[10–14] pressure,[15–18] strain,[19] torque,[20] and moisture level[21,22]) using passive sensors (no embedded battery source) probed using a wireless radio frequency (rf) link. The basic sensor principle is based on disturbing the resonance frequency of a rf resonator.[23] We actually use surface acoustic wave (SAW) devices made of a piezoelectric substrate—quartz in all the examples described here—patterned with electrodes for receiving and emitting electromagnetic waves converted to acoustic waves through the piezoelectric effect.[24]

We are interested on the one hand in operating a low frequency device due to the better penetration of electromagnetic waves in dielectric substrates such as the ones the parts being monitored are made of, as well as to the ease of the fabrication of the sensors made of larger patterns when operating at lower frequency. On the other hand, high frequency provides the means for reducing the sensor and antenna sizes.

Since we aim at complying with rf emission regulations, two main frequency bands are usable in Europe: 434 and 2450 MHz. The latter frequency band is wide enough for the operation of acoustic reflective delay lines (so-called SAW tags[25–32]), but the penetration depth of the electromagnetic wave is too poor to embed the sensor in most dielectric substrates such as soil or polymers. We are hence interested in the 434 MHz band, which however only provides a 1.7 MHz bandwidth, insufficient for interrogating delay lines with dimensions smaller than 10 mm but allowing for SAW-resonator-based sensor exploitation.[33–36]

Hence, we focus on an interrogation unit[37] allowing the identification of the resonance frequency of narrowband acoustic devices: resonators. Since we will focus on the interrogation instrument, we will assume the availability of resonators with acoustic modes operating within the 434

a)Electronic mail: jmfriedt@femto-st.fr.

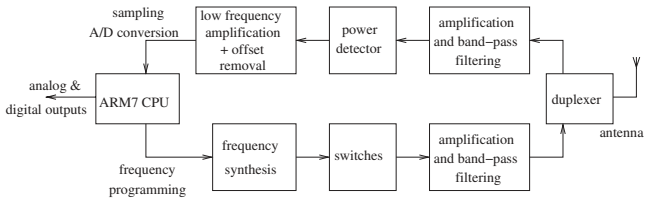

FIG. 1. General strategy of the narrowband wireless acoustic sensor interrogation unit.

MHz band, with quality factors in the 10000 ± 2000 range; our objective is the identification of these resonance frequencies using means compatible with a wireless link, and the conversion of these frequencies to the physical parameter affecting the resonator (Fig. 1).

The strategy we have first selected for interrogating narrowband devices is a slow sweep of a frequency source with a spectral response narrower than that of the resonator. This strategy is similar to that used by network analyzers, although the wireless link induces an additional constraint, namely, the alternating emission and reception phases, similar to that used in radar systems. The basic components we need are, hence, a versatile frequency source, a rf power reception circuit, and switches for activating and deactivating emission and reception phases during the interrogation cycles. We have selected a fully software-controlled strategy in which a central ARM7 (Ref. 38) microcontroller synchronizes all the interrogation steps, from the frequency generation to the digitization of the rf power level and postprocessing of the spectra for identifying the resonance frequencies.

II. SENSOR DESIGN

Piezoelectric sensors provide an efficient means of storing energy transferred through a rf link. Being intrinsically rf components, SAW resonators are compact and do not require additional components for converting the measured quantity to a rf signal, even though such schemes have been demonstrated with, for example, resonance frequency pulling by a capacitive sensor.[34,39]

SAW resonators built on single crystal piezoelectric substrates exhibit parametric sensitivities varying along the substrate's crystal orientation and are, hence, suitable for the design of temperature or stress sensors (and associated pressure and torque sensors). In order to reduce the sensitivity of SAW to unwanted parameters, and to reduce requirements on the local reference oscillator (Sec. III A), we exploit a differential design in which the frequencies of a reference resonator and a sensing resonator are both monitored.[40,41] This particular sensor provides usable signals in the −20–150 °C range while keeping all resonances within the 1.7 MHz ISM band range; the typical first order temperature coefficient of frequency (TCF) is thus of the order of 10 kHz/°C (23 ppm/K). This TCF is practically reduced to 2.5 kHz/°C (6 ppm/K) to account for the differential measurement which is performed under the assumption of the ISM band division in two equal parts and including manufacturing variability; this value will be used throughout this article.

This simple dual-resonator design, however, lacks the ability to identify the sensor; both resonances are used for the measurement, and optimum resolution is achieved by using all the available rf band for the measurement. Adding a resonance for an identification step would strongly reduce the measurement accuracy; in all the following discussion, the interrogation unit is only associated to a single sensor at any given measurement time.

III. FREQUENCY GENERATION

Generating rf signals with continuously tunable frequency is commonly performed by two major techniques: frequency multiplication using a phase locked loop and mixing.[42] Both methods are compatible with a software control of the emitted frequency using a quartz-controlled direct digital synthesizer (DDS). A 32-bit frequency control word generating a 34 MHz signal to be mixed with a 400 MHz reference provides subhertz accuracy, below the long term stability of the local reference oscillator.

In order to reduce the number of components and the possible noise sources, we select a DDS (Analog Devices AD9954) strategy in which the core clock f_{ck} is naturally added to the output frequency f_{out} due to the basic principle of DDS components. This output is bandpass filtered using a SAW filter and amplified to reach the maximum allowed output power of 10 dBm as measured during continuous emission. The need for mixing is, hence, eliminated and the major phase noise source—the 400 MHz signal—is eliminated so that the only phase noise source remains the oscillator powering the DDS (Fig. 2).

The phase noise of such a synthesis was measured at 435 MHz and provided the best performance in the frequency range of interest—100 Hz–10 kHz from the carrier frequency—when compared to a mixing strategy (400 MHz PLL output mixed with 35 MHz DDS output) or a PLL multiplication strategy (54.375 MHz DDS output multiplied by 8).

A. Local oscillator stability issue

All timing signals are synthesized from a unique quartz crystal resonator. Typical crystal oscillators provide ±10–±50 ppm stability over the industrial temperature range (−40 to 85 °C), i.e., 0.2–0.8 ppm/K. In a single resonator configuration, the resonance frequency change of the sensor is smaller than this reference oscillator noise; a temperature sensor working over a 170 K range and complying with the 434 MHz band ISM regulations displays a linear coefficient of 23 ppm/K, so that a 0.1 K accuracy requires a local oscillator accuracy better than 3 ppm/K. Below such stability, the drift of the reference oscillator cannot be distinguished from the frequency shift of the sensor due to a temperature variation during a measurement; common reference oscillator drift is not negligible with respect to the measured frequency variation associated with the physical quantity measurement.

One aspect of dual resonators including a reference is that the local oscillator drift affects the measurement of both resonance frequencies; although the available ISM band frequency range is halved, the frequency shift to be measured is now in the megahertz range (half of the available ISM band) rather than close to 434 MHz. The requirements on the local

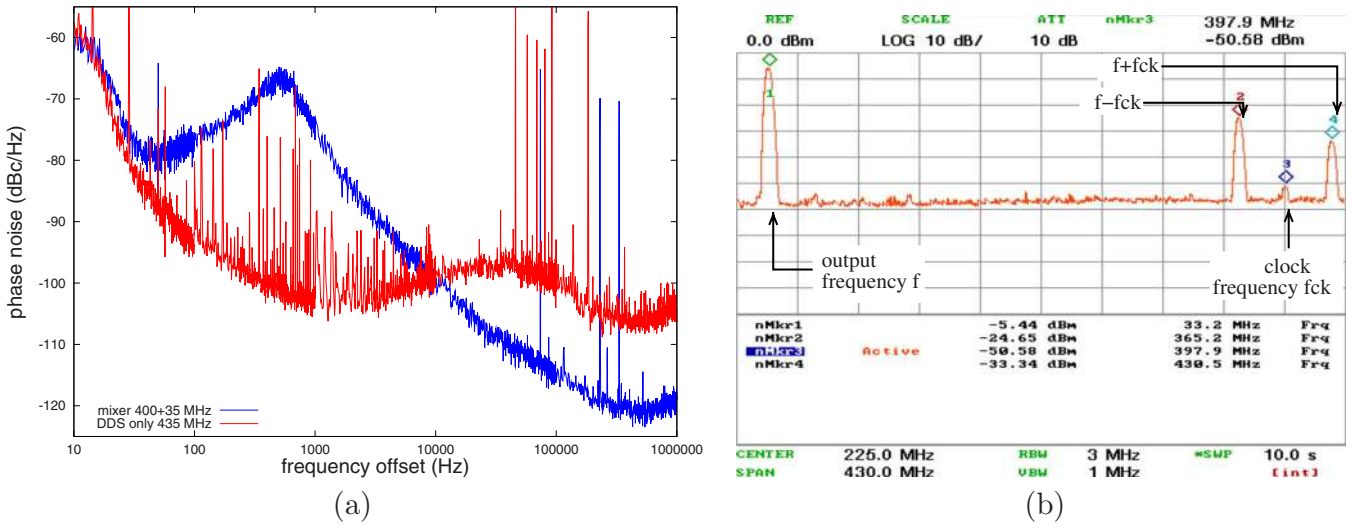

FIG. 2. (Color online) (a) Comparison of the phase noises of 435 MHz signals obtained by mixing a 400 MHz signal resulting of a PLL multiplication of a 20 MHz source and a 35 MHz output of a DDS clocked by this same 20 MHz source internally multiplied to 400 MHz, and by the bandpass filtered 435 MHz output of this same DDS resulting from the intrinsic generation of a signal at a frequency, which is the sum of the clock and output signal frequencies. (b) Raw output of the AD9954 DDS clocked at $f_{ck}=400$ MHz and programmed to output a frequency $f=33$ MHz. The 400+33 MHz output is bandpass filtered using two SAW filters and amplified to 0 dBm for generating the rf probe pulse.

oscillator stability are, hence, reduced to about 670 ppm over the temperature range, easily met by any commercially available resonator. Furthermore, aging is assumed to affect in a similar trend both resonators so that the difference frequency is hardly affected, while a single resonator measurement requires periodic recalibration to assess aging associated drift.

On the other hand, if a single resonator scheme is selected, means of long term stabilization of the local oscillator (GPS 1 PPS signal,[43,44] NTP timing protocols over the internet[45]) are necessary to preserve the measurements accuracy over long time periods. Furthermore, we have observed[46] that frequency pulling due to antenna impedance variations associated with the interrogation unit environment changes significantly affects a single resonance, while under the assumption that in a two resonator setup both resonators exhibit the same impedance, such pulling is eliminated during the differential measurement step.

IV. RADIO FREQUENCY POWER RECEPTION

A. Power reception

Wideband Identity/Quadrature (I/Q) demodulators and power detectors are commercially available with cutoff frequencies well above 434 MHz. We use such detectors—for example Analog Devices AD8362—for direct power measurement after filtering and amplifying the signal received by the antenna, switched toward the reception circuit. The bandpass filtering is performed by a bandpass SAW filter so as to reject any signal outside the ISM band. However, integrating the total power within the whole ISM band makes the detector sensitive to unwanted signals, since unwanted emitters in the ISM band, which provide a signal as strong as the returned signal from the loaded resonator, mask the wanted signal. Furthermore, the rf receiver noise level increases with increasing reception frequency bandwidth. We have nevertheless observed that the 60 dB dynamic range is enough to reach an interrogation range of several meters (typically 3 m, 11 m at best) in free space.

An alternative scheme providing efficient demodulation and improved resistance to unwanted emitters, yet keeping the 60 dB dynamic range, is the use of I/Q demodulators, such as Analog Devices AD8302. The output of either magnitude signal from the I/Q demodulator or power detector is fed to a fast, rail to rail operational amplifier configured as amplifier and subtractor for removing any offset generated by the rf stage. The output of the operational amplifier is directly connected to the fast analog to digital converter of the microcontroller (1 Msample/s). The control of all sequences by this same processor guarantees the best synchronization of the switch commutation followed by a fast sampling of the received power; the resulting magnitude is associated with the frequency that was programmed in the DDS during this same sequence. No frequency uncertainty between a slowly, continuously, varying voltage controlled oscillator and the sampling time is introduced with this scheme. A 1 Msample/s analog to digital converter is fast enough to process the power detector output of a 434 MHz resonator with a quality factor Q of 10 000 since the decay time after loading the resonator is Q/π periods, equal to about 6 μs. This scheme is, however, no longer applicable to higher frequency resonators (with lower Q-factor assuming a constant $Q\times f$ product) since the decay duration scales with the square of the resonance frequency f. The 1 μs threshold occurs at 1 GHz, above which a fast sample and hold amplifier is necessary, again triggered by the same microcontroller in charge of controlling the whole measurement process.

B. Interrogation range improvement

Including a 1–32 dB programmable attenuator in the emission chain (before the power amplifier and the duplexer

to which the antenna is connected) increases the range dynamics close to the interrogation unit by avoiding signal saturation on the receiver stage as would occur when emitting at full power. This aspect is fundamental since most applications require the interrogation unit to probe the SAW sensor at distances ranging from a few centimeters to a meter at most.

A digital automatic-gain-control providing a command to the attenuator proportional to the received signal strength has revealed robust to most environments in which the sensor is continuously viewed by the interrogation unit. Improved resistance to unwanted emitters is provided by a listen-before-talk mechanism; before emitting a new pulse toward the SAW sensor, the power received by the interrogation unit is compared with an upper threshold, above which we consider that an unwanted emitter is occupying the required frequency band.

V. SIGNAL PROCESSING TECHNIQUES

Reduced frequency sweep durations require a limited number of sampling frequencies. A tradeoff has to be found between fast sampling (the response at few frequencies are sampled) and the resolution with which the resonance frequency is identified (requiring the response at many frequencies for high resolution). Here, a different approach is used to improve the resolution of the resonance frequency identification; using digital signal processing—and more specifically polynomial fit of the resonance shape—is used to improve the precision of the resonance frequency location.[28] We describe here a criterion for selecting the frequency step based solely on the quality factor of the resonator, and we deduce the corresponding resolution improvement. Furthermore, the algorithmic simplicity of the scheme is compatible with any low grade 32-bit central processing unit since only two arithmetic operations (one division and one multiplication) are needed.

The sampling of the interrogation signal frequency is set accounting for the resonance Q to ensure that at least three frequencies are within the bandpass of the resonator. For resonators centered around $f \simeq 434$ MHz and $Q=10\,000$, the frequency step is 14.5 kHz; the whole 1.7 MHz wide ISM band requires 117 sampling frequencies interrogation sequences according to the above criterion.

As the emission pulses must be narrower than the spectral width of the resonator, each emission pulse must exhibit a bandwidth close to $f/Q=40$ kHz; each pulse must last at least 25 μs. Considering that the processing time, data storage, and programming of the next DDS frequency step takes another 30 μs, each interrogation (i.e., frequency sampling) lasts 60 μs and an ISM-band sweep requires about 7.5 ms.

117-point accuracy over the whole range is a sensor whose resolution can be considered as 7-bit accurate, and in this case the temperature of the sensor is identified with a 1.5 K resolution; we wish to improve this resolution by using a resonance frequency determination exploiting the whole envelope of the resonance shape rather than simply the maximum for instance. As a reference, we wish to improve the resolution beyond that of Maxim's DS1621, a 9-bit digital temperature sensor working over a similar temperature range, based on a similar concept of comparing the frequencies of two resonators with different TCF.[47]

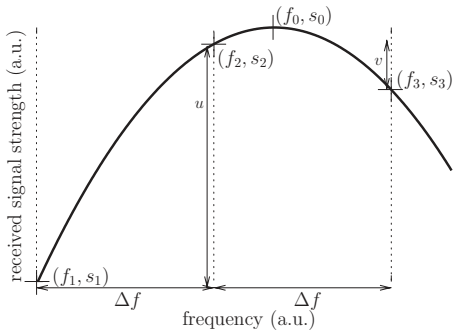

FIG. 3. Three measurements of the received signal magnitude s_1, s_2, and s_3 at three probe frequencies f_1, f_2, and f_3, respectively, are fitted using a second order polynom in order to identify the true resonance frequency f_0.

By using a second order polynomial fit of the resonance, using not only the frequency of the maximum returned signal but also its two neighbors, we provide a computationally efficient algorithm for improving the accuracy of the resonance frequency estimation by a factor equal to the signal to noise ratio of the detected signal, as will now be demonstrated.

A. Resonant frequency identification improvement

Once the returned signal has been sampled for all frequencies in the ISM band with a constant frequency step Δf, the response thus acquired is processed for the identification of the resonance frequency; rather than selecting the point for which the returned signal is maximum, we will apply a parabolic fit on the point of maximum returned signal (frequency f_2 for which the maximum returned signal is s_2) and its two neighbors (f_1,s_1) and (f_3,s_3) with $f_1=f_2-\Delta f$, $f_3=f_2+\Delta f$, and $s_1<s_2$, $s_3<s_2$ (Fig. 3). This parabolic fit is justified as a second order Taylor development of the "true" returned signal shape, which includes the Butterworth-van Dyke (BvD[48,49]) response of the resonator associated with parasitic elements of the packaging and rf link.

The position f_0 of the maximum of the parabola running through these three points (f_1,s_1), (f_2,s_2), and (f_3,s_3) is then given, by computing the abscissa at which the derivate of the polynom becomes 0, by

$$f_0 = f_2 + \frac{\Delta f}{2} \times \frac{s_1 - s_3}{s_1 + s_3 - 2 \times s_2}.$$

An uncertainty analysis on this formula, developed by assuming Δf and f_2 perfectly known (no error on the sampled frequencies generated by the DDS), states that the uncertainty on the resonance frequency correction $d(f_0-f_2)$ is dependent upon the noise on the received signal measurement and the height difference between the sampled amplitudes,

$$d(f_0 - f_2) = \frac{\Delta f}{(u+v)^2} \times (|v|du + |u|dv),$$

where $u=s_1-s_2$ and $v=s_3-s_2$ (Fig. 3) and du, dv the uncertainties on these two quantities.

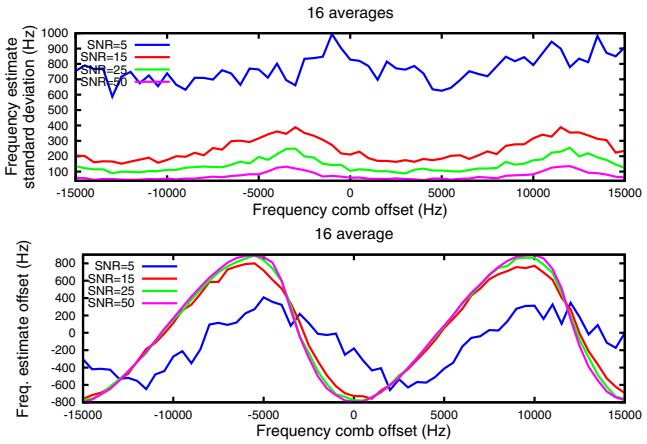

FIG. 4. (Color online) Top: comparison of a BvD model (L_1=72.8 μH, C_1=1.85 fF, R_1=21 Ω, and C_0=3.3 pF) and the parabolic fit around resonance f_0, in the frequency domain in the range $f_0 \pm \Delta f_0/(3Q)$. Bottom: zoom on this same frequency region, with the display of the error between the model and the parabolic approximation in percent.

In the case where $u \simeq v$ and $du \simeq dv$ (the case $u \neq v$ is discussed in Fig. 4), then this formula simplifies to

$$d(f_0 - f_2) \simeq \frac{du}{2|u|}\Delta f.$$

Hence, an optimum value of Δf is established as a trade-off between maximizing $s_3 - s_2$ and $s_2 - s_1$, i.e., using a large Δf, and keeping the parabolic approximation accurate, i.e., keeping Δf small enough (as defined later) to keep f_1 and f_3 close to the true resonance frequency f_0 for the second order Taylor development to be valid. Numerical simulation on a BvD model of the resonator response shows that the error between a polynomial fit of the conductance and the true resonance shape differ by less than $\pm 1\%$ if $\Delta f \leq f_0/3 \times Q$ (Fig. 5); this

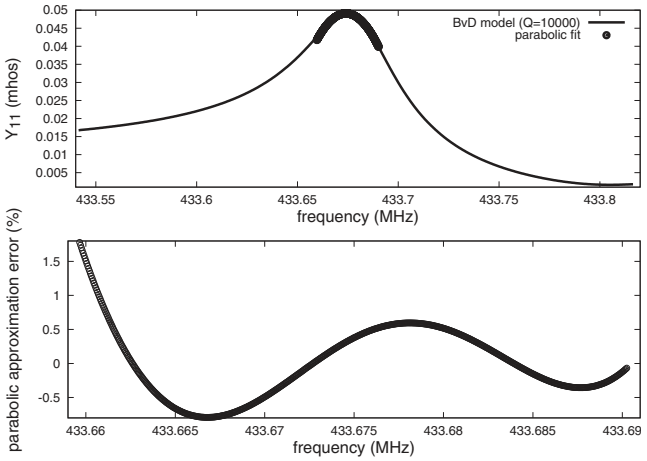

FIG. 5. Monte Carlo simulations of noisy reflected signal magnitude following a BvD model (L_1=72.8 μH, C_1=1.85 fF, R_1=21 Ω, and C_0=3.3 pF) yielding a theoretical resonance frequency of 433 674 982 Hz and a quality factor around 9500, consistent with available sensor characteristics. With these values, Δf=15.3 kHz. The standard deviation and bias of the estimated frequency f_0 to the true resonance frequency are maximum when the resonance frequency is in the middle of two frequencies of the comb, and are minimum when one frequency of the comb matches the resonance frequency. In this simulation, the frequency comb was centered on 433 679 185 Hz, i.e., an offset of 4202 Hz to the true resonance frequency of the device.

value will be used throughout the remaining discussion. Considering the signal to noise ratio of the magnitude measurements of the signal reflected by the resonator, improvements by a factor $du/2|u| \geq 16$ is commonly observed, yielding a sensor with 12-bit accuracy over the whole measurement range.

B. Influence of the parabolic approximation of the resonance shape

We analyze now the influence of the second order Taylor development of the resonance shape, and especially the effect of the position of f_2 with respect to f_0. When the resonator is probed with a frequency comb at $f_2 \pm N\Delta f$, N integer, the assumption that $u \simeq v$ is only correct if $f_2 = f_0$, while it becomes inaccurate when $s_1 \simeq s_2$ or $s_3 \simeq s_2$ which happens when $f_0 \simeq f_2 \pm \Delta f/2$. Since we use a fixed frequency comb, while f_0 continuously shifts with the varying physical quantity, each case mentioned above will occur during an experiment. We must, hence, identify the error induced by the parabolic fit approximation when f_0 moves from $f_2 - \Delta f/2$ to $f_2 + \Delta f/2$; this analysis is performed numerically.

We consider that the returned signal as a function of frequency follows a BvD shape (Fig. 5, whose caption provides the parameter used for the simulations). We perform simulations in which a uniformly distributed random noise is added to the returned signal (equivalent to the noise associated with du and dv in the previous discussion, Sec. V A), and run the parabolic fit analysis mentioned previously on these noisy data. We iterate multiple times (100 times) this simulation procedure and compute the average and standard deviation on the estimates of f_0. Our reference for comparison is the value of f_0 identified by sampling with 1 Hz step the modeled BvD admittance response.

Simulations (Fig. 5) confirm experimental observations (Fig. 6) that the standard deviation of the resonance frequency estimate is dependent on the position of the comb with respect to the resonance; if one frequency of the comb is located on f_0, the lowest standard deviation is observed, while the maximum standard deviation is observed when f_0 is located at the middle between two frequencies of the comb, namely, $f_2 \pm \Delta f/2$ (Fig. 5). The bias between the true resonance frequency (f_0 estimated by extracting the maximum of the conductance from the BvD model) and fitted frequency is at most 800 Hz or, with classical temperature coefficients of the resonator, an equivalent temperature bias of 0.32 °C.

Temperature accuracies better than this value can be achieved by moving the frequency comb so that one of its frequencies (f_2) matches the true resonant frequency f_0 of the sensor estimated from the last measurement. The digital control of the whole rf synthesis chain allows for such dynamic feedback algorithm to be used with minimal computational power requirements as will be explained in the next section.

C. Frequency tracking strategy

Since each frequency is generated by the DDS independently of the previous one, versatile strategies can be

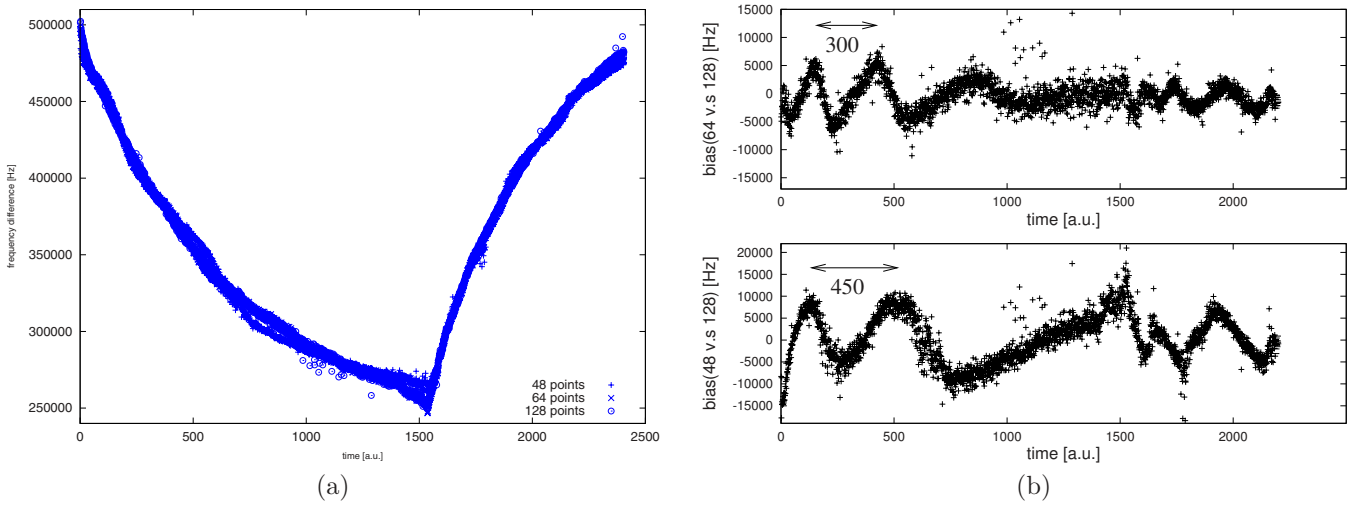

FIG. 6. (Color online) Bias on the estimated resonance frequency difference experimentally observed during a sensor heating and cooling experiment (top): the ISM band was scanned with 48, 64, and 128 steps. Although the general trend and the average value are independent of the number of sampled frequencies in the ISM band, the bias associated with the parabolic shape are clearly observed, and magnified on the bottom curve by subtracting the curve with highest sampling rate (128, assumed to be representative of the actual heating and cooling kinetic) from the two other curves (64 and 48 sampled frequencies). Note that the distance between the first two bias maxima are separated by a distance scaling with the number of sampled frequencies: 450/300=64/48, in agreement with our interpretation of the origin of the bias associated with the spacing between the frequencies of the comb.

adapted. For example, we have demonstrated numerically that the lower noise level and bias is observed when one frequency of the spectral comb probing the sensor coincides with the resonance frequency of the resonator (i.e., where the assumption $u \simeq v$ is verified). Adapting the frequency comb position is thus mandatory for a maximum accuracy of the resonance frequency evaluation. Furthermore, when the sensor is always visible from the interrogation unit, faster (as defined later) strategies focusing only on the frequencies close to the last identified resonance position have been implemented; although providing greater information update rates since only six frequencies are probed (f_0 and $f_0 \pm \Delta f$ for both the reference and measurement resonators) instead of 117 (hence an information update rate improved $117/6 \simeq 20$ times), loss of signal will render this algorithm inefficient since a full sweep of the ISM range is needed to reassess f_0. This frequency tracking strategy has appeared less robust in most practical situations where external rf perturbations or signal loss occur (see Appendix for further details).

D. Further signal processing: Averaging

We have experimentally established that—as expected for a random Gaussian noise on the estimate of the resonance frequency—the standard deviation on the frequency measurements decreases as the square root of the number of averaged data. Hence, unless a particular application requires a fast sampling rate (vibration measurement for example, requiring a bandwidth above 10 Hz), we average 16 successive resonance frequency estimates—a tradeoff between the information update rate to the user and standard deviation improvement efficiency when reaching the asymptotic behavior of the averaging process—and, hence, reduce the standard deviation from 300 Hz for individual measurements to 75 Hz after averaging, as observed during experiments aimed at probing a SAW sensor through a 26 dB attenuator for a controlled rf link. The drawback of averaging is the lower sampling rate; in that case, the measurement duration is 7.5 $\times 16 = 120$ ms.

A 75 Hz standard deviation on the measured difference of the resonance frequencies provides a temperature measurement for this sensor with standard deviation 30 mK, although dependent upon the rf link quality; the temperature standard deviation is often increased to 0.25 K when the SAW sensor is interrogated through a wireless link since in that case, the additional thermal and electromagnetic noise brought by the antenna raises the noise level above the 75 Hz level.

VI. RESULTS AND APPLICATIONS EXAMPLES

We assess experimentally the strategy described so far by interrogating a SAW sensor designed for the measurement of temperature. The TCF of this dual resonator sensor is 2500 Hz/K (6 ppm/K) as defined earlier (see Sec. II). The two aims of these measurements are the following:

- the estimation on a static sensor of the resolution of the measurement, i.e., the assessment of the various causes of noise and bias on the resonance frequency measurements as the sensor is constantly seen by the interrogation unit, and
- the estimation of the minimum duration during which a sensor must be visible from the interrogation unit to perform a measurement, and hence the maximum speed at which a mobile object supporting the sensor might move with respect to the static interrogation electronics. In that case, we assume that the sensor is periodically visible from the interrogation unit in order to perform successive averages even though the sensor is not constantly accessible via the rf link (as is the case on a rotating object such as a motor axis or a wheel).

The current implementation of the strategies described

so far has been implemented with sampling the ISM frequency range with 128 points (more than the required 117 points for digital computation efficiency), with frequency steps of 13.3 kHz. The emission duration is selected so that the corresponding power spectrum is narrower than the resonator resonance; with an experimental Q at 434 MHz around 10 000, we select an emission duration of 30 μs. The signal processing duration and DDS programming step require another 30 μs, for a total ISM sweep 7.5 ms long. As explained previously, we perform 16 averages to reduce the frequency detection standard deviation below 200 Hz, so the physical quantity measurement is updated every 120 ms. The samples of the average do not need to be contiguous; we accumulate samples until either the wanted number of samples is reached, or a timeout is reached. The resulting algorithm is stable even with sensors only intermittently visible to the interrogation antenna. The requirement is that the sensor is seen by the interrogation antenna at least 7.5 ms; this condition is met on a 30 cm radius wheel rotating at 37 Hz (2600 rpm or 300 km/h driving speed) when the visibility angle is 120°. The antenna, hence, is of utmost importance when interrogating sensors located on a rotating object; the greater the angular coverage of the interrogation and sensor antennas, the higher the speed at which the rotating sensor will be usable.

The influence of the number of sampled frequencies within the ISM band Δf_{ISM} on the measurement accuracy is experimentally assessed as illustrated in Fig. 6. Although a small number of sampled frequencies is suitable to increase the measurement rate (and hence reduce the needed visibility duration of the sensor, or increase the motion velocity of the sensor with respect to the fixed interrogation antenna), too small a number n $n(n \ll \Delta f_{\mathrm{ISM}} \times 3Q/f_0)$ yields a bias on the measurement associaated with the non-parabolic shape of the resonance. This bias is experimentally observed and defines the minimum number of sampled frequencies: we typically sample 128 frequencies within the 434 MHz ISM band (13,3 kHz steps).

VII. CONCLUSION

We have demonstrated the use of a versatile system for the wireless interrogation of passive SAW sensors in the 434 MHz frequency range inspired from radar techniques. A full software control of all interrogation steps—from the emitted signal frequency to duplexer switching between emission and reception stages and rf power magnitude sampling—provides the means to implement various strategies for probing the resonant frequency of resonating sensors. Signal processing strategies such as the interrogation scheme presented here reduce the number of sampled frequencies so that the interrogation steps are compatible with a sensor visible by the interrogation unit for less than 10 ms, as is typically seen on rotating objects such as wheels or rotating axis in industrial applications. These signal processing steps, if not properly modeled and understood, might yield unwanted measurement artifacts as was demonstrated theoretically and experimentally. Finally, it turns out that a simple versatile interrogation electronics reveals particularly adapted for testing various strategies and rf link protocols able to improve wireless sensing system features. Different approaches will be further tested in that matter.

ACKNOWLEDGMENTS

The authors acknowledge fruitful discussions with L. Fagot-Revurat (MFPM, France).

APPENDIX: REDUCING FREQUENCY BIAS BY AVERAGING BEFORE FITTING

One aspect associated with digital signal processing and the bias induced by the parabolic fit of the received signals is to identify the origin of the bias and whether a better processing technique might remove it. Here we are modeling the parabolic fit on noisy data generated from a three points along a parabola $y=-x^2$ $(x=\{x_0;x_0+1;x_0+2\}$ and $x_0 \in [-1.5:-0.5])$ to which a uniformly distributed noise

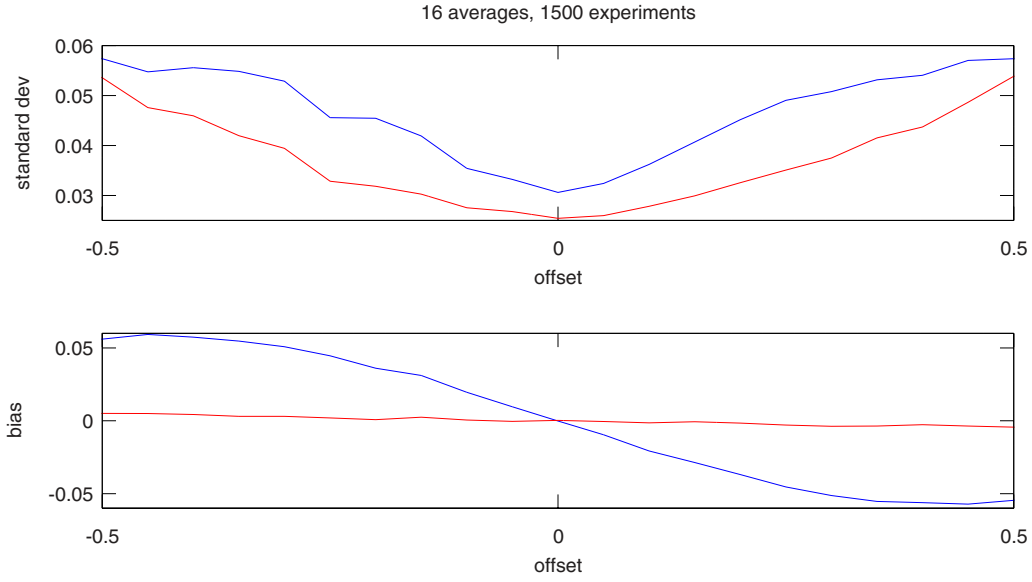

FIG. 7. (Color online) Standard deviation and bias of the estimated parabola maximum as a function of the position of f_1, f_2, and f_3 with respect to the true maximum $f_0=0$. Here $\Delta f=1$.

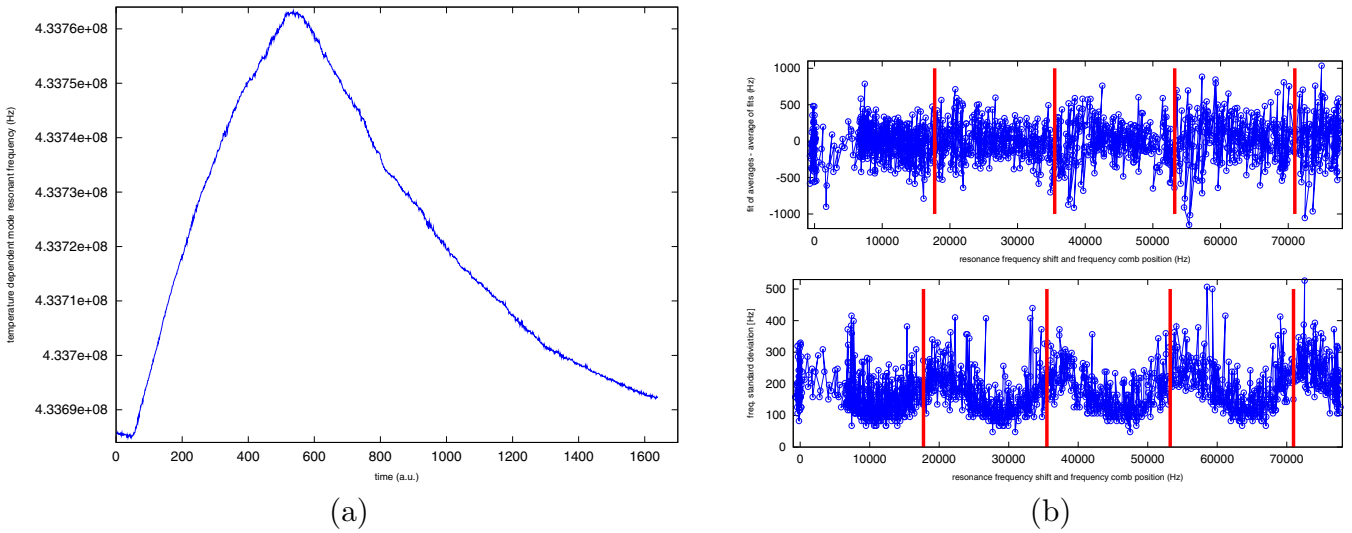

FIG. 8. (Color online) (a) Time evolution of a temperature sensitive resonance as the sensor is heated by a 2 A current running through a 1 Ω resistor. (b) Top: experimental measurement of the difference between the resonance position maximum estimated by averaging 16 parabola maxima measured on noisy data on the one hand, and estimating from a single parabola fit on 16 measurement averages on the second hand. The bold vertical lines are spaced by a frequency comb spacing (Δf=17.74 kHz in this example) and show that indeed the maximum noise level is observed with such a periodicity. (b) Bottom: experimental measurement of the standard deviation of the 16 frequencies accumulated for computing each sample in the parabola maxima averaging strategy. The red lines are spaced by a frequency comb spacing (Δf=17.74 kHz in this example) and show that indeed the maximum noise level is observed with such a periodicity.

in the $[-0.5:0.5]$ range is added. We then plot the position of the estimated parabola maximum as a function of two processing algorithms:

(1) first fitting the noisy data with a parabolic fit, identifying the position of the maximum of this fitted parabola, and after accumulating 16 estimates, averaging the estimates to deduce the resonance position, and
(2) averaging multiple (16) noisy measurements for averaging, and performing a single parabolic fit on the averaged data.

Not only is the second strategy more efficient in terms of computational power (only one multiplication is needed instead of the 16 multiplications for each iteration of the first algorithm), but Fig. 7 shows that the standard deviation on 1500 simulations is lower or equal for the second algorithm compared to the first one, but most significantly that the bias is strongly reduced by first averaging the raw measurements followed by the parabolic fit instead of averaging the results of the fits.

One interesting aspect of Fig. 7 is that the bias of the estimated resonance frequency to the true frequency is not associated with the approximation due to the second order Taylor development of the resonance shape but is intrinsic to fitting noisy measurements along the parabola and averaging multiple maxima position estimates. This theoretical result is confirmed by experimental measurements (Fig. 8); in this experiment, a dual resonator is connected through a 23 dB attenuator to the rf output of the interrogation unit. The resonance frequency of both resonance and measurement modes are monitored using either an averaging (16 values) of each resonance position estimated following a polynomial fit (i.e., average of the frequency position), or a single parabolic on the average of the returned signals.

The first algorithm is nevertheless used for mobile sensor probing since each measurement is individually validated for incorporation in the average following a threshold criterion; this identification of the presence of the sensor in view of the interrogation unit is not possible when all ISM frequency sweep results are accumulated for later parabolic fitting analysis.

[1] T. Liu, C. Sadler, P. Zhang, and M. Martonosi, MobiSYS'04, 2004.
[2] L. Krishnamurthy, R. Adler, P. Buonadonna, J. Chhabra, M. Flanigan, N. Kushalnagar, L. Nachman, and M. Yarvis, Proceedings of the Third International Conference on Embedded Networked Sensor Systems, 2005, pp. 64–75.
[3] X. Conghui, G. Peijun, C. Wenyi, T. Xi, Y. Na, and M. Hao, J. Semicon. **30**, 045003 (2009).
[4] N. Cho, S.-J. Song, S. Kim, S. Kim, and H.-J. Yoo, Proceedings of the 31st Solid-State Circuits Conference, 2005, pp. 279–282.
[5] P. Pursula, J. Marjonen, H. Ronkainen, and K. Jaakkola, *Transducers and Eurosensors'07* (Lyon, France, 2007), pp. 73–76.
[6] T. Nomura, A. Saitoh, and H. Tokuyama, in WCU (2003), pp. 935–938.
[7] Y. Dong, W. Cheng, S. Wang, Y. Li, and G. Feng, Sens. Actuators B **76**, 130 (2001).
[8] G. Scholl, F. Schmidt, T. Ostertag, L. Reindl, H. Scherr, and U. Wolff, IEEE International Frequency Control Symposium, 1998, pp. 595–601.
[9] A. Springer, R. Weigel, A. Pohl, and F. Seifert, Mechatronics **9**, 745 (1999).
[10] F. Schmidt, O. Sczesny, L. Reindl, and V. Mhgori, IEEE Ultrasonics Symposium, 1994, pp. 589–592.
[11] G. Bruckner, R. Hauser, A. Stelzer, L. Maurer, L. Reindl, R. Teichmann, and J. Biniasch, Proceedings of the 2003 IEEE International Frequency Control Symposium and PDA Exhibition, Jointly with the 17th European Frequency and Time Forum, 2003, pp. 942–947.
[12] W. Bulst, G. Fischerauer, and L. Reindl, IEEE Trans. Ind. Electron. **48**, 265 (2001).
[13] L. Reindl and I. Shrena, IEEE Trans. Ultrason. Ferroelectr. Freq. Control **51**, 1457 (2004).
[14] S. Schuster, S. Scheiblhofer, L. Reindl, and A. Stelzer, IEEE Trans. Ultrason. Ferroelectr. Freq. Control **53**, 1177 (2006).
[15] H. Scherr, G. Scholl, F. Seifert, and R. Weige, IEEE Ultrasonics Symposium, 1996, pp. 347–350.
[16] A. Pohl, G. Ostermayer, L. Reindl, and F. Seifert, IEEE Ultrasonics Symposium, 1997.

[17] A. Pohl and L. Reindl, Advanced Microsystems for Automotive Applications Conference, 1998, pp. 250–262.
[18] H. Oh, W. Wang, K. Lee, I. Park, and S. Yang, International Journal on Smart Sensing and Intelligent Systems **1**, 940 (2008).
[19] A. Pohl, R. Steindl, and L. Reindl, IEEE Trans. Instrum. Meas. **48**, 1041 (1999).
[20] J. Beckley, V. Kalinin, M. Lee, and K. Voliansky, IEEE International Frequency Control Symposium and PDA Exhibition, 2002, pp. 202–213.
[21] M. Dierkes and U. Hilleringmann, Advances in Radio Science **1**, 131 (2003).
[22] A. Stelzer, G. Schimetta, L. Reindl, A. Springer, and R. Weigel, SPIE Proceedings—Subsurface and Surface Sensing Technologies and Applications III, 2001, Vol. 4491, pp. 358–366.
[23] J. H. Kuypers, M. Esashi, D. A. Eisele, and L. M. Reindl, IEEE Ultrasonics Symposium, 2006, pp. 1453–1458.
[24] R. White and F. Voltmer, Appl. Phys. Lett. **7**, 314 (1965).
[25] A. Pohll, F. Seifert, L. Reind, G. Scholl, T. Ostertag, and W. Pietschl, IEEE Ultrasonics Symposium, 1994, pp. 195–198.
[26] L. Reindl, G. Scholl, T. Ostertag, C. Ruppel, W.-E. Bulst, and F. Seifert, IEEE Ultrasonics Symposium, 1996, pp. 363–367.
[27] R. Brocato, Sandia Report pp. 1–20 (2006).
[28] L. Reindl, Proceedings of the Second International Symposium on Acoustic Wave Devices for Future Mobile Communication Systems, 2004, pp. 1–15.
[29] X. Q. Bao, W. Burkhard, V.V. Varadan, and V. Varadan, IEEE Ultrasonics Symposium, 1987, pp. 583–585.
[30] C. Hartmann, Proceedings of 2002 IEEE Ultrasonics Symposium, 2002.
[31] C. S. Hartmann, P. Brown, and J. Bellamy, Proceedings of the Second International Symposium on Acoustic Wave Devices for Future Mobile Communication Systems (2004).
[32] P. Hartmann, IEEE International Conference on RFID, 2009, pp. 291–297.
[33] W. Buff, F. Plath, O. Schmeckebier, M. Rusko, T. Vandahl, H. Luck, F. Möller, and D. Malocha, IEEE Ultrasonics Symposium, 1994, pp. 585–588.
[34] T. Osterag and S. Kunzmann, IQ-mobil Gmbh pp. 1–9 (2003).
[35] A. Pohl, G. Ostermayer, and F. Seifert, IEEE Trans. Ultrason. Ferroelectr. Freq. Control **45**, 1061 (1998).
[36] Y. Wen, P. Li, J. Yang, and M. Zheng, IEEE Sens. J. **4**, 828 (2004).
[37] A. Stelzer, R. Hauser, L. Reindl, and R. Teichmann, Proceedings of the 17th IMEKO World Congress, 2003, pp. 672–675.
[38] S. Segars, K. Clarke, and L. Gourdge, IEEE MICRO **15**, 22 (1995).
[39] R. Matsuzaki and A. Todoroki, Sens. Actuators, A **119**, 323 (2005).
[40] W. Buff, S. Klett, M. Rusko, J. Ehrenpfordt, and M. Goroli, IEEE Trans. Ultrason. Ferroelectr. Freq. Control **45**, 1388 (1998).
[41] W. Buff, M. Rusko, M. Goroll, J. Ehrenpfordt, and T. Vandahl, IEEE Ultrasonics Symposium, 1997, pp. 359–362.
[42] A. Stelzer, S. Schuster, and S. Scheiblhofer, International Workshop on SiP/SoC Integration of MEMS and Passive Components with RF-ICs, 2004.
[43] F. Cordara and V. Pettiti, Proceedings of the 27th Precise Time and Time Interval (PTTI) Applications and Planning Meeting, 1995, pp. 113–124.
[44] W. Lewandowski, P. Moussay, P. Guerin, F. Meyer, and M. Vincent, Proceedings of the11th European and Time Forum (EFTF), 1997, pp. 493–497.
[45] K. Kalliomaki, T. Mansten, and A. Rautiainen, Joint IEEE International Frequency Control Symposium with the 21st European Frequency and Time Forum, 2007, pp. 865–867.
[46] G. Martin, P. Berthelot, J. Masson, W. Daniau, V. Blondeau-Patissier, B. Guichardaz, S. Ballandras, and A. Lamber, IEEE Ultrasonics Symposium, 2005, Vol. 4, pp. 2089–2092.
[47] Maxim Application Note 127 (2001).
[48] D. Dye, Proc. Phys. Soc. London **38**, 399 (1925).
[49] K. V. Dyke, Phys. Rev. **25**, 895 (1925).